Title
Bladder tissue regeneration using acellular bi-layer silk scaffolds in a large animal model of augmentation cystoplasty

Journal
Biomaterials, 34(34)

ISSN
0267-6605

Authors
Tu, Duong D
Chung, Yeun Goo
Gil, Eun Seok
et al.

Publication Date
2013-11-01

DOI
10.1016/j.biomaterials.2013.08.001

Peer reviewed

Published in final edited form as:
Biomaterials. 2013 November ; 34(34): . doi:10.1016/j.biomaterials.2013.08.001.

Bladder Tissue Regeneration Using Acellular Bi-Layer Silk Scaffolds in a Large Animal Model of Augmentation Cystoplasty

Duong D. Tu[1,2,*], **Yeun Goo Chung**[1,*], **Eun Seok Gil**[3], **Abhishek Seth**[1,2], **Debra Franck**[1], **Vivian Cristofaro**[2,4,5], **Maryrose P. Sullivan**[2,4,5], **Dolores Di Vizio**[1,2,6], **Pablo Gomez III**[1,2], **Rosalyn M. Adam**[1,2], **David L. Kaplan**[3], **Carlos R. Estrada Jr.**[1,2,§], and **Joshua R. Mauney**[1,2,§]

[1]Urological Diseases Research Center, Boston Children's Hospital, Boston, MA 02115, USA

[2]Department of Surgery, Harvard Medical School, Boston, MA 02115, USA

[3]Department of Biomedical Engineering, Tufts University, Medford, MA, 02155, USA

[4]Division of Urology, Veterans Administration Boston Healthcare System, Boston, MA 02132, USA

[5]Department of Surgery, Brigham and Women's Hospital, Boston, MA 02115, USA

[6]Samuel Oschin Comprehensive Cancer Institute, Cedars-Sinai Medical Center, 8700 Beverly Boulevard, Los Angeles, CA 90048

Abstract

A cellular scaffolds derived from *Bombyx mori* silk fibroin were investigated for their ability to support functional tissue regeneration in a porcine model of augmentation cystoplasty. Two bi-layer matrix configurations were fabricated by solvent-casting/salt leaching either alone (Group 1) or in combination with silk film casting (Group 2) to yield porous foams buttressed by heterogeneous surface pore occlusions or homogenous silk films, respectively. Bladder augmentation was performed with each scaffold group ($6\times6cm^2$) in juvenile Yorkshire swine for 3 m of implantation. Augmented animals exhibited high rates of survival (Group 1: 5/6, 83%; Group 2: 4/4, 100%) and voluntary voiding over the course of the study period. Urodynamic evaluations demonstrated mean increases in bladder capacity over pre-operative levels (Group 1: 277%; Group 2: 153%) which exceeded non surgical control gains (144%) encountered due to animal growth. Similarly, elevations in bladder compliance were substantially higher in augmented animals from baseline (Group 1: 357%; Group 2: 147%) in comparison to controls (41%). Gross tissue evaluations revealed that both matrix configurations supported extensive *de novo* tissue formation throughout the entire original implantation site which exhibited ultimate tensile strength similar to nonsurgical counterparts. Histological and immunohistochemical analyses showed that both implant groups promoted comparable extents of smooth muscle regeneration and contractile protein (α-smooth muscle actin and SM22α) expression within defect sites similar to controls. Parallel evaluations demonstrated the formation of a transitional, multi-layered urothelium with prominent cytokeratin, uroplakin, and p63 protein expression in both matrix groups. *De novo*

[§]Corresponding authors: Joshua R. Mauney, Ph.D., Boston Children's Hospital, Department of Urology, John F. Enders Research Laboratories, 300 Longwood Ave., Rm. 1009, Boston, MA 02115, USA; Phone: 617-919-2521; Fax: 617-730-0248; joshua.mauney@childrens.harvard.edu; Carlos Estrada, M.D., Boston Children's Hospital, Department of Urology, 300 Longwood Ave., Hunnewell 3, Boston, MA 02115, USA; Phone: 617-355-3338; Fax: 617-730-0474; carlos.estrada@childrens.harvard.edu.
[*]Equal contribution

innervation and vascularization processes were evident in all regenerated tissues indicated by synaptophysin-positive neuronal cells and vessels lined with CD31 expressing endothelial cells. *Ex vivo* organ bath studies demonstrated that regenerated tissues supported by both silk matrices displayed contractile responses to carbachol, α,β-methylene-ATP, KCl, and electrical field stimulation similar to controls. Our data detail the ability of acellular silk scaffolds to support regeneration of innervated, vascularized smooth muscle and urothelial tissues within 3 m with structural, mechanical, and functional properties comparable to native tissue in a porcine model of bladder repair.

Keywords

silk; tissue engineering; bladder; wound healing

1. Introduction

Enterocystoplasty is the primary surgical procedure utilized to reduce urinary storage pressures and reduce the risk of renal damage and incontinence associated with a variety of congenital and acquired bladder pathologies including neurogenic bladder, bladder exstrophy, and posterior urethral valves [1,2]. Transposition of gastrointestinal segments into the urinary tract leads to a number of significant complications including chronic urinary tract infection, metabolic abnormalities, secondary malignancies, as well as donor site morbidity [3,4], all of which can compromise the efficacy of the treatment and adversely affect the patient's quality of life. Short-term clinical studies of bladder tissue engineering have investigated both natural and synthetic scaffolds either alone or seeded with autologous bladder cell populations as alternative strategies for defect repair or neobladder reconstruction [5,6]. In particular, Atala et al. first demonstrated the ability of a biodegradable, collagen-coated poly-glycolic acid (PGA) mesh, seeded with autologous cells expanded *ex vivo*, to mediate *de novo* bladder tissue formation in children afflicted with myelomeningocele [5]. However, bladder compliance and capacity failed to increase in the majority of subjects to a clinically relevant degree potentially compromising the long-term effectiveness of this approach to mitigate the high intravesical pressures routinely encountered in this patient population [7].

Previous reports have demonstrated that incorporation of autologous primary cells into scaffolds prior to implantation enhances the ability of tissue engineered constructs to mediate bladder tissue repair [8–10]. However this strategy harbors practical and technical concerns which may hamper its widespread clinical deployment. First, the use of patient-derived cells requires secondary surgical procedures for tissue isolation and propagation of *in vitro* cultures [5], thereby requiring substantial laboratory resources to attain sufficient cell numbers for implant seeding. In addition, urothelial and smooth muscle cells are subject to de-differentiation during *in vitro* cultivation [11,12], potentially compromising the *in vivo* performance of seeded constructs. Moreover, autologous cells isolated from diseased bladders have been shown to display various functional abnormalities [13,14] and therefore may not be suitable for restoration of normal organ operations. The risk of pathogen acquisition prior to re-implantation is also a significant safety concern associated with this approach [15]. Recent clinical trials deploying decellularized small intestinal submucosa (SIS) grafts for augmentation cystoplasty in exstrophy patients sought to overcome limitations associated with cell-seeded approaches for bladder reconstruction [6]. However, implantation of acellular SIS matrices failed to establish long-term urinary continence and did not support significant increases in bladder capacity and compliance as well as regeneration of normal smooth muscle architecture. Therefore, there is a significant need to

develop alternative, acellular biomaterial configurations with the capacity to promote functional bladder tissue regeneration.

Biomaterials derived from *Bombyx mori* silkworm cocoons exhibit a unique set of properties including high structural strength and elasticity [16], diverse processing plasticity [17], and tunable biodegradability [18] which make them particularly suited for the repair of hollow organ defects. Previous studies in rodent models of augmentation cystoplasty have demonstrated that acellular silk scaffolds display particular advantages in comparison to conventional PGA and SIS scaffolds including improved functional performance, enhanced tissue regeneration, and minimal inflammatory reactions [19,20]. In particular, a bi-layer scaffold configuration, comprised of a porous silk foam buttressed by a nonpermeable silk layer, supported the formation of innervated, vascularized bladder tissue while promoting significant increases in bladder capacity and compliance [20]. In the current study, we investigated the ability of acellular bi-layer silk scaffolds to mediate tissue regeneration in a porcine model of bladder augmentation.

2. Materials and Methods

2.1. Biomaterials

Aqueous silk fibroin solutions were prepared from *B. mori* silkworm cocoons [16] and utilized to construct two bi-layer matrix configurations using methods previously described [16,20]. For Group 1 matrices, a 6% wt/vol silk fibroin solution was mixed with sieved granular NaCl (500–600 μM, average crystal size) in a ratio of 2 g NaCl per ml of silk solution and cast within a rectangular vessel for 48 h at 37°C. Group 2 scaffolds were produced similarly; however the NaCl/silk solution was layered on to a silk film which was generated first by drying a 8% wt/vol silk solution within the casting vessel for 48 h at room temperature under a laminar flow hood. NaCl was subsequently removed from both matrix variants by washing the scaffolds for 72 h in distilled water with regular volume changes. Scaffold groups were then autoclave sterilized and subjected to analytical or surgical procedures described below.

2.2. Scanning electron microscopy (SEM)

Structural analysis of matrix groups prior to implantation was performed in order to assess differences in scaffold morphology generated by various fabrication techniques. Matrix samples were sputter coated with Pt/Pd and imaged using a Zeiss scanning electron microscope, model EVO MA10 (Carl Zeiss AG, Germany).

2.3. Porcine augmentation cystoplasty

Bladder augmentation was performed in 10 juvenile female Yorkshire swine (3 m of age) following IACUC-approved protocols. Three additional pigs served as longitudinal controls receiving no surgical intervention. Open and robotic-assisted laparoscopic augmentation cystoplasty were utilized for scaffold implantation in independent animals in order to verify the efficacy of the bi-layer scaffolds to be used in both traditional open and minimally-invasive laparoscopic surgical procedures. Both surgical approaches were performed under sterile technique with maintenance anesthesia using 2–3% isoflurane following induction with intramuscular injection of 0.4mg/kg atropine, 2.2mg/kg xylazine, and 4.4mg/kg tiletamine+zolazepam. All pigs were mechanically ventilated for the duration of the operative procedures.

Augmentation cystoplasty was performed via a hand-assisted robotic approach (Group 1: N=2) as previously described [21]. Briefly, the dome of the bladder was incised longitudinally, and a $6\times6cm^2$ scaffold was introduced via a hand port and anastomosed to

the bladder defect using a 3-0 polyglactin suture in a running fashion. Marking sutures were placed at all 4 corners of the scaffold with a 4-0 polypropylene nonabsorbable suture. Open augmentation cystoplasty was also performed (Group 1: N=4; Group 2: N=4) as previously described [22]. Briefly, a lower abdominal midline incision was made and carried down through the peritoneum to expose the bladder. The bladder dome was opened longitudinally and scaffolds ($6\times6 cm^2$) were anastomosed and bordered by marking sutures as described for the robotic technique. For both surgical approaches, a urethral catheter was advanced into the bladder lumen and secured to the perineum. Organ distension via the urethral catheter was performed with saline infusion following scaffold integration to ensure no gross leaks were present through the scaffold center or along the suture line. Rectus abdominis fascia and skin incisions were subsequently closed with running sutures. The urethral catheter was left free to drainage for 7 d post-implantation in all augmented animals. Following catheter removal, animals were allowed to void voluntarily. All animals were kept on prophylactic antibiotics (3.3 mg/kg/d nitrofurantoin) for 8 d post-operatively. Urethral recatheterization and additional antibiotic treatment of two animals implanted with Group 1 scaffolds was performed respectively at 1 m and 2 m post-operatively for 2 wk due to the presence of low-grade fevers. After this period, catheters were removed and animals were allowed to void voluntarily until the completion of the study. Analysis of serum creatinine levels was performed in all animals pre-operatively and at 1, 2, 3 m post-operatively. Nonsurgical controls and swine receiving implants were euthanized at 3 m post-implantation and isolated bladder specimens were subjected to contractile, histological and immunohistochemical, and mechanical analyses.

2.3. Urodynamics

Bladder compliance and capacity were determined pre-operatively and at 3 m post-implantation under anesthesia. Longitudinal nonsurgical swine were evaluated in parallel upon arrival into the animal housing facility and following 3 m of boarding. Briefly, a 12 French urethral catheter was inserted into the bladder and attached to two 3-way stopcocks arranged in series. One stopcock was attached to a glass manometer which was maintained level with the animal's bladder and the other was used for instillation of contrast agent (Optiray™, Hazelwood, MO) at 37°C. Stepwise cystometry was performed as previously described [23] wherein intravesical pressure measurements were recorded at 50 ml increments up to 1650 ml instilled volume. Bladder capacity and cystogram images were recorded at a fill volume exerting ~20 cmH_2O pressure to avoid organ rupture or vesicoureteral reflux. Bladder compliance was determined by calculating Δvolume/Δpressure between ~10–20 cmH_2O during cystometry.

2.4. Mechanical testing

Uniaxial tensile tests were performed as previously described [24] on an Instron 3366 testing frame (Norwood, MA) equipped with a 100 N capacity load cell and Biopuls pneumatic clamps. Scaffold specimens prior to implantation (N=4 per group) as well as regenerated (3 m post-operatively) and control tissues harvested from the bladder dome (N=3–4 per group) were hydrated in phosphate buffered saline (PBS) at least 3 h to reach a swelling equilibrium prior to testing. Test samples were submerged in a temperature-controlled testing container (Biopuls) filled with PBS at 37°C. A displacement control mode with a crosshead displacement rate of 1.8 mm/min was used, and the gauge length was 10 mm. The initial elastic modulus (EM), ultimate tensile strength (UTS) and % elongation to failure (ETF) were calculated from stress/strain plots. EM was calculated by using a least-squares (LS) fit within the linear elastic region. UTS was determined as the highest stress value attained during the test and the ETF was the last data point before a >10% decrease in the load. Data were presented as mean ± standard deviation.

2.5. Histological and immunohistochemical analyses

Regenerated and control tissue segments from both the periphery and central regions of the bladder dome were excised for standard histological processing. Briefly, specimens were fixed in 10% neutral-buffered formalin, dehydrated in graded alcohols, and then embedded in paraffin. Sections (10 μm) were cut and then stained with hematoxylin and eosin (H&E). For immunohistochemical (IHC) analyses, contractile smooth muscle markers such as α-smooth muscle actin (α-SMA) and SM22α; urothelial-associated protein, uroplakin (UP), cytokeratins (CK), and p63; neuronal and endothelial markers, synaptophysin (SYP38) and CD31, respectively, were detected using the following primary antibodies: anti-α-SMA [Sigma-Aldrich, St. Louis, MO, cat.# A2457, 1:200 dilution], anti-SM22α [Abcam, Cambridge, MA, cat.# ab14106, 1:200 dilution], anti-pan-UP [rabbit antisera raised against total bovine UP extracts, 1:100 dilution], anti-pan-CK [Dako, Carpinteria, CA, cat.# M3515, 1:200 dilution], anti-p63 [Santa Cruz Biotechnology, Santa Cruz, CA, cat.# sc-8431, 1:200 dilution], anti-SYP38 [Abcam, cat.# ab8049, 1:200 dilution], anti-CD31 [Abcam, cat.# ab228364, 1:100 dilution]. Sections were then incubated with species-matched Cy3-conjugated secondary antibodies (Millipore, Billerica, MA) and nuclei were counterstained with 4', 6-diamidino-2-phenyllindole (DAPI). Specimens were visualized using an Axioplan-2 microscope (Carl Zeiss MicroImaging, Thornwood, NY) and representative images were acquired using Axiovision software (version 4.8).

2.6. Ex vivo contractility

Regenerated tissue segments harvested from the central bladder dome of the original defect site as well as native tissues extracted from similar regions of longitudinal controls were subjected to *ex vivo* organ bath contractility analyses as previously described [25]. Briefly, bladder tissue strips either intact or separated from mucosa were suspended in an organ bath maintained at 37°C and bubbled with a mixture of 95% O_2 and 5% CO_2. Tissues were attached to a force transducer (Grass Instruments), stretched to a resting tension of 2 g and equilibrated for 45 min. Contractile responses to carbachol (cholinergic agonist, 1 nM–10 μM), α,β-methylene (me)-ATP (purinergic agonist, 10 μM), KCl (120 mM), and to electrical field stimulation (EFS) (1–64 Hz, 20 V, 0.5 ms pulse width, 10 sec duration) were measured. Conditioned signals from force transducers were continuously acquired at 30 Hz by a 16-channel analog-to-digital converter (DataQ, DI-720) and recorded to disk using Windaq data acquisition software. Data were expressed as force (mN) normalized by tissue cross-sectional area and presented as mean ± standard deviation.

2.6. Statistical analyses

Tensile testing and contractility measurements were analyzed with the Mann-Whitney U test using SPSS Statistics software v19.0 (www.spss.com). Statistically significant values were defined as $p<0.05$.

3. Results and Discussion

SEM analyses of scaffold groups (Figure 1A) revealed the formation of a bi-layer structure with distinct structural compartments. The solvent-cast/NaCl-leached layer comprised the bulk of each scaffold variant and resembled a foam configuration with large pores (pore size, ~400μm) interconnected by a network of smaller pores dispersed along their periphery. Group 1 scaffolds displayed spontaneous pore occlusion of the solvent-cast/NaCl-leached layer along the plane adjacent to the casting vessel; however continuity of this feature was heterogeneous along the surface area with pockets of porous channels. In contrast, Group 2 matrices were buttressed by a homogenous, non porous silk film (200μm thick) generated by the annealing of dehydrated silk solutions during casting.

Tensile testing of matrix groups prior to implantation (Figure 1B) revealed that Group 2 scaffolds displayed significantly higher UTS (2.4-fold) and EM (3.6-fold) in comparison to Group 1. These features suggest that the presence of the annealed silk film in Group 2 matrices acted to reinforce the foam compartment, therefore substantially increasing global construct mechanical integrity. However, ETF values were found to be similar between the two matrix configurations regardless of the presence of the annealed silk film therefore providing evidence that the overall flexibility of the bi-layer scaffolds is primarily influenced by the properties of the foam compartment. Indeed, comparisons between ETF of Group 2 scaffolds (44%) and a similar matrix variant (197%) previously utilized for rat bladder augmentation [20], wherein the foam compartment was considerably thinner (33% of Group 2), but with a comparable film layer, revealed an inverse correlation between overall construct ETF and foam compartment thickness. Taken together, these results highlight the contribution of each scaffold layer to overall construct tensile properties.

Robot-assisted laparoscopic and open augmentation cystoplasty were both feasible approaches for surgical integration of bi-layer silk scaffolds into bladder defects (Figure 2A–C). Over the course of the 3 m implantation period, the survival rate of augmented animals receiving Group 1 or 2 scaffolds was 83% (5/6) and 100% (4/4), respectively, prior to scheduled euthanasia. Exploratory laparotomy following the one animal death occurring in Group 1 at 2 d post-op revealed urinary ascites as the probable cause of death. Despite leak testing immediately following bladder integration, prominent fluid leaks throughout the center of the scaffold were observed during post-mortem saline instillation of the augmented bladder. The inability of this Group 1 replicate to support integrity of the defect site was presumably due to unstable pore occlusion of the bulk foam matrix following implantation. In contrast, no signs or symptoms of urinary ascites were seen over the course of the study period in any of the animals implanted with Group 2 scaffolds. This observation suggests that the annealed silk film compartment in the Group 2 matrix configuration confers a particular advantage in maintaining defect consolidation over Group 1 scaffolds as a whole.

Urodynamic studies (Figure 3A) showed a wide extent of pre-operative bladder capacities (range, 250–1050 ml; median, 425 ml) in all subjects analyzed (12/13) independent of initial animal weight (mean, 37.2 ± 3.3 kg). Non surgical longitudinal controls demonstrated substantial elevations in bladder capacity (144%) and overall weight (41%) following the 3 m study period, consistent with juvenile animal growth. Swine implanted with Group 1 or 2 matrices exhibited similar increases in overall weight (Group 1: 40%; Group 2: 33%); however at 3 m post-op, respective gains in bladder capacity were substantially higher in comparison to controls with levels of 277% and 153% over baseline. Qualitative expansion of bladder size following 3 m post-op was confirmed by cystography in subjects implanted with both silk groups (Figure 3B). No evidence of contrast extravasation in the reconstructed organs was noted.

In contrast to bladder capacity, pre-operative bladder compliance for all animals investigated (12/13) was similar with a mean value of 34 ± 6 ml/cmH_2O. Longitudinal controls displayed a 41% increase in bladder compliance following 3 m of housing consistent with published observations showing a positive correlation between this parameter and growth during juvenile stages of development [26]. In comparison to compliance gains in controls, animals implanted with both matrix configurations demonstrated considerably higher mean differentials over baseline levels with increases of 357% and 147% in Groups 1 and 2, respectively. These results are consistent with our previous urodynamic study in rats wherein a 10-fold increase in organ compliance was observed following bladder augmentation with bi-layer silk scaffolds [20]. Interestingly, augmentation cystoplasty in this rodent model with SIS or structurally-divergent gel spun silk scaffolds led to modest 1.5-fold increases in this parameter. Collectively, these data demonstrate that regenerative

processes supported by bi-layer silk scaffolds selectively promote increases in organ compliance in both small and large animal models of bladder repair. This feature is potentially advantageous for clinical bladder reconstruction since increases in bladder compliance are desired in patients afflicted with neurogenic bladder or exstrophy which often display reduced levels of this parameter [27] elevating the risk for high intravesical pressures and subsequent renal damage.

Following 3 m post-op, gross tissue evaluations of the upper urinary tract revealed no signs of hydronephrosis or renal anomalies in controls or animals implanted with either silk matrix configuration. These results are consistent with the lack of significant alterations in serum creatinine levels in all experimental groups over the course of the study (data not shown) suggestive of normal kidney function. In all augmented bladders, extensive host tissue ingrowth spanned the entire area of the original implantation site with a midline scar apparent in each regenerated tissue which was more prominent in Group 2 subjects (Figure 4A, B). Negligible contraction between the anterior to posterior lengths of the original implanted areas was observed between the marking sutures following defect consolidation with both scaffold types. In contrast, prominent lateral contraction was noted in all implantation sites regardless of the matrix configuration utilized. Tensile testing (Figure 4C) revealed that the regenerated tissues in both implant groups displayed UTS similar to controls. However, the EM of the consolidated tissues from Group 1 and 2 was elevated in comparison to native levels by 1.6-fold and 3-fold, respectively, indicating an increase in stiffness. In addition, implantation of Group 1 and 2 scaffolds led to *de novo* tissue formation which exhibited respective ETF values which were 80% and 46% of control levels.

In 3/4 animals augmented with Group 2 scaffolds, intravesical urinary calculi were observed (Figure 4B, insert) which varied in appearance from encrusted films reminiscent of annealed silk layers utilized during scaffold construction to soft, amorphous sedimentous debris. Analysis of all Group 2 calculi revealed a calcium carbonate/calcium phosphate (95/5%) composition. In subjects implanted with Group 1 matrices, stone formation was minimal and specific to only 1/5 animals with a composition similar to those observed in Group 2. The increase in stone formation in swine implanted with Group 2 matrices is presumably due to the relatively slow degradation kinetics of the annealed silk film layer in comparison to the bulk foam compartment. Indeed, our previous study in rodents demonstrated that nonporous silk films comprising bi-layer silk scaffolds remained largely intact and were a nidus for stone formation following bladder augmentation [20]. These results are consistent with other published studies which demonstrate the extent of scaffold porosity is a significant factor in determining the rate of degradation presumably due to more efficient exposure of the matrix interior to proteolytic enzymes and subsequent polymer hydrolysis [18,24]. Future scaffold optimization studies will focus on increasing the rate of *in vivo* degradation of annealed silk films through pre-treatment with proteolytic enzymes prior to implantation; an approach previously shown to enhance degradation kinetics [28].

Global histological examinations (H&E analysis) at 3 m post-op revealed that in both experimental groups there was extensive ingrowth of connective tissue from the host bladder wall into both the radial peripheral and central regions of the original implantation sites (Figure 5). In addition, cross-sectional organization throughout the *de novo* bladder wall in each augmented group resembled native control tissue architecture with distinct compartments consisting of a lumenal epithelium, an extra-cellular matrix (ECM)-rich lamina propria, and an outer layer of smooth muscle bundles. H&E analysis also revealed discrete regions of mild fibrosis dispersed throughout the central and radial peripheral regions of all regenerated tissues with exception of the midline scar area present in both groups wherein moderate levels of fibrosis were detected (data not shown). Throughout all

regenerated tissues supported by both scaffold groups, discrete areas of chronic inflammatory reactions were observed with mobilized follicular aggregates of mononuclear cell infiltrates. Similarly, minimal acute inflammatory reactions characterized by the presence of occasional eosinophil granulocytes were also noted (data not shown). These immunogenic responses are similar to those previously observed in rodent models of bladder augmentation with silk biomaterials [24]. In addition, extensive fragmentation of the porous compartment of both scaffold configurations was noted within the regenerated lamina propria with qualitatively higher levels of residual scaffold remnants present within the central bladder wall in comparison to the radial peripheral areas. These data suggest that degradation of the bi-layer scaffolds proceeded in a radial fashion from the border of the original implantation site toward the center regions as host tissue integration proceeded.

IHC assessments revealed that the reconstituted smooth muscle layers in both experimental groups stained positive for α-SMA and SM22α contractile protein expression to similar extents as those observed in control specimens indicating prominent smooth muscle maturation (Figure 6A). A cytokeratin-positive, multi-layer urothelium was also present within both radial peripheral and central regions of the regenerated tissues supported by each matrix configuration (Figure 6B). The transitional nature of the urothelium was confirmed in all regenerated tissues by IHC analysis wherein p63-positive basal and intermediate cell layers were lined with lumenal p63-negative superficial cells. Varying degrees of hyperplasia were observed in the basal and intermediate cell compartments supported by Group 2 scaffolds in comparison to controls. This feature may reflect incomplete urothelial maturation since normalization of basal/intermediate cell proliferation is required during wound healing for native tissue stratification to be achieved [24,29]. Regenerated tissues supported by both scaffold types displayed robust UP expression in both superficial and intermediate cell layers to levels similar to those observed in control tissues. Expression and assembly of UP into heterodimers which form asymmetrical unit membranes is essential for maintaining the integrity of the urothelial permeability barrier [30].

Evidence of *de novo* vascularization and innervation processes were observed throughout all regenerated tissues supported by each implant group (Figure 6C). Vessels containing prominent CD31 positive endothelial cells were found in both the radial periphery and central implantation sites while neuronal lineages displaying SYP38 indicative of synaptic transmission areas were localized throughout the *de novo* bladder wall. These results demonstrate that silk scaffold configurations described in this study are capable of supporting regeneration of innervated, vascularized smooth muscle and urothelial tissues in a large animal model of bladder repair.

Detrusor smooth muscle contractility is an integral process mediating voiding function in the bladder. Contractility analyses of isolated bladder muscle strips were performed to ascertain the ability of the scaffold groups to support functional regeneration. Carbachol-induced contractile responses in denuded bladder strips demonstrated statistically similar extents of tensile force in tissues from both augmented groups in comparison to control levels over all steady-state drug concentrations examined (Figure 7A). These data suggest that the regenerated smooth muscle displays muscarinic receptor-mediated contractile responses since carbachol is a known agonist of muscarinic receptors which have been reported to mediate bladder contraction in swine [31]. Comparisons between regenerated bladders strips with intact mucosa from both augmented groups and their denuded counterparts showed a significant reduction in tensile force in response to carbachol stimulation (data not shown). This feature is consistent with published reports demonstrating an inhibitory effect of the mucosa on carbachol-induced contraction of porcine bladder smooth muscle [32] and therefore shows the regenerated mucosa from both implant groups displayed this type of bioactivity.

Contractile responses to nerve stimulation following EFS [33] were also observed in denuded bladder strips from both control and regenerated tissues indicating functional innervation in the augmented groups (Figure 7B). However, EFS (2–32 Hz) produced significantly reduced levels of tensile force in Group 2 bladder strips in comparison to controls while Group 1 specimens responded similarly to native tissue across all frequencies tested. Induction of smooth muscle contractility by KCl-mediated membrane depolarization demonstrated similar degrees of tensile force generated by regenerated tissues from both implants groups in comparison to control levels (Figure 7C), indicating the integrity of the contractile apparatus in regenerated tissues. In addition, the generation of tensile forces following α,β-methylene-ATP stimulation in *de novo* tissues supported by each scaffold group provides evidence for postsynaptic purinoceptor activation and contractility responses following tissue regeneration (Figure 7D). Collectively, these data show that silk scaffolds support regeneration of bladder smooth muscle tissue with contractile properties in a porcine defect model.

4. Conclusions

The results presented in this study detail the ability of acellular silk scaffolds to support regeneration of innervated, vascularized smooth muscle and urothelial tissues with structural, mechanical, and functional properties comparable to native controls in a porcine model of bladder repair. In addition, our data show implantation of these matrices promoted gains in bladder capacity and compliance over pre-operative and control levels as well as voluntary animal voiding. Performance comparisons between silk matrix configurations demonstrate that reinforcement of porous silk foams with annealed silk films present in Group 2 scaffolds increases overall matrix UTS and EM and enhances animal survival by reducing the incidence of organ leakage following defect consolidation. Optimization of silk film layers in Group 2 matrices through modulation of fabrication procedures will be a future goal in order to reduce the incidence of stone formation and translation potential of this scaffold technology toward clinical applications. In addition, verification of the efficacy of silk matrices to recapitulate the results of this study in animal models of bladder disease is a requirement before patient deployment will be considered. In any event, this report provides a foundation for further investigations into the potential of silk scaffolds for functional tissue engineering of clinical-scale urinary tract defects.

Acknowledgments

Suzanne White and the staff at the Histology Core Facility at Beth Israel Deaconess Medical Center, Boston, MA are acknowledged for technical assistance with tissue processing for histological analyses. This research was supported by theTissue Engineering Resource Center, NIH/NIBIB P41 EB002520 (KAPLAN); NIH/NIDDK P50 DK065298 (ADAM); NIH/NIDDK T32-DK60442 (FREEMAN); NIH/NCI R00 CA-131472 (Di VIZIO); NIH/NIDDK R00 DK083616-01A2 (MAUNEY)

References

1. Guys JM, Hery G, Haddad M, Borrionne C. Neurogenic bladder in children: basic principles, new therapeutic trends. Scand J Surg. 2011; 100:256–263. [PubMed: 22182847]
2. Biers SM, Venn SN, Greenwell TJ. The past, present and future of augmentation cystoplasty. BJU Int. 2012; 109:1280–1293. [PubMed: 22117733]
3. Scales CD Jr, Wiener JS. Evaluating outcomes of enterocystoplasty in patients with spina bifida: a review of the literature. J Urol. 2008; 180:2323–2329. [PubMed: 18930285]
4. Husmann DA, Rathbun SR. Long-term follow up of enteric bladder augmentations: the risk for malignancy. J Pediatr Urol. 2008; 4:381–385. [PubMed: 18653384]
5. Atala A, Bauer SB, Soker S, Yoo JJ, Retik AB. Tissue-engineered autologous bladders for patients needing cystoplasty. Lancet. 2006; 367:1241–1246. [PubMed: 16631879]

6. Caione P, Boldrini R, Salerno A, Nappo SG. Bladder augmentation using acellular collagen biomatrix: a pilot experience in exstrophic patients. Pediatr Surg Int. 2012; 28:421–428. [PubMed: 22350082]
7. Kropp BP, Zwischenberger JB. Tissue-engineered autologous bladders: new possibilities for cystoplasty. Nat Clin Pract Urol. 2006; 3:588–589. [PubMed: 17088926]
8. Yoo JJ, Meng J, Oberpenning F, Atala A. Bladder augmentation using allogenic bladder submucosa seeded with cells. Urology. 1998; 51:221–225. [PubMed: 9495701]
9. Oberpenning F, Meng J, Yoo JJ, Atala A. *De novo* reconstitution of a functional mammalian urinary bladder by tissue engineering. Nat Biotechnol. 1999; 17:149–155. [PubMed: 10052350]
10. Lai JY, Chang PY, Lin JN. Bladder autoaugmentation using various biodegradable scaffolds seeded with autologous smooth muscle cells in a rabbit model. J Pediatr Surg. 2005; 40:1869–1873. [PubMed: 16338308]
11. Flieger A, Golka K, Schulze H, Follmann W. Primary cultures of human urothelial cells for genotoxicity testing. J Toxicol Environ Health A. 2008; 71:930–935. [PubMed: 18569598]
12. Chamley-Campbell J, Campbell GR, Ross R. The smooth muscle cell in culture. Physiol Rev. 1979; 59:1–61. [PubMed: 108688]
13. Hipp JA, Hipp JD, Yoo JJ, Atala A, Andersson KE. Microarray analysis of bladder smooth muscle from patients with myelomeningocele. BJU Int. 2008; 102:741–746. [PubMed: 18336610]
14. Subramaniam R, Hinley J, Stahlschmidt J, Southgate J. Tissue engineering potential of urothelial cells from diseased bladders. J Urol. 2011; 186:2014–2020. [PubMed: 21944117]
15. Bolin SR, Matthews PJ, Ridpath JF. Methods for detection and frequency of contamination of fetal calf serum with bovine viral diarrhea virus and antibodies against bovine viral diarrhea virus. J Vet Diagn Invest. 1991; 3:199–203. [PubMed: 1655059]
16. Kim UJ, Park J, Kim HJ, Wada M, Kaplan DL. Three-dimensional aqueous-derived biomaterial scaffolds from silk fibroin. Biomaterials. 2005; 26:2775–2785. [PubMed: 15585282]
17. Altman GH, Diaz F, Jakuba C, Calabro T, Horan RL, Chen J, et al. Silk-based biomaterials. Biomaterials. 2003; 24:401–416. [PubMed: 12423595]
18. Wang Y, Rudym DD, Walsh A, Abrahamsen L, Kim HJ, Kim Hs, et al. *In vivo* degradation of three-dimensional silk fibroin scaffolds. Biomaterials. 2008; 29:3415–3428. [PubMed: 18502501]
19. Mauney JR, Cannon GM, Lovett ML, Gong EM, Di Vizio D, Gomez P 3rd, et al. Evaluation of gel spun silk-based biomaterials in a murine model of bladder augmentation. Biomaterials. 2011; 32:808–818. [PubMed: 20951426]
20. Seth A, Chung YG, Gil ES, Tu D, Franck D, Di Vizio D, et al. The performance of silk scaffolds in a rat model of augmentation cystoplasty. Biomaterials. 2013; 34:4758–4765. [PubMed: 23545287]
21. Kang IS, Lee JW, Seo IY. Robot-assisted laparoscopic augmentation ileocystoplasty: a case report. Int Neurourol J. 2010; 14:61–64. [PubMed: 21120178]
22. Merguerian PA, Reddy PP, Barrieras DJ, Wilson GJ, Woodhouse K, Bagli DJ, et al. Acellular bladder matrix allografts in the regeneration of functional bladders: evaluation of large-segment (>24 cm) substitution in a porcine model. BJU Int. 2000; 85:894–898. [PubMed: 10792173]
23. Clementson Kockum C, Willén R, Malmfors G. Bladder augmentation with different forms of intestinal grafts: an experimental study in the pig. BJU Int. 1999; 83:305–311. [PubMed: 10233500]
24. Gomez P 3rd, Gil ES, Lovett ML, Rockwood DN, Di Vizio D, Kaplan DL, et al. The effect of manipulation of silk scaffold fabrication parameters on matrix performance in a murine model of bladder augmentation. Biomaterials. 2011; 32:7562–7570. [PubMed: 21764119]
25. Seth A, Chung YG, Kim D, Ramachandran A, Cristofaro V, Gomez P 3rd. The impact of discrete modes of spinal cord injury on bladder muscle contractility. BMC Urol. 2013; 13:24. [PubMed: 23668225]
26. Wahl EF, Lerman SE, Lahdes-Vasama TT, Churchill BM. Measurement of bladder compliance can be standardized by a dimensionless number: theoretical perspective. BJU Int. 2004; 94:8957.
27. Schaefer M, Kaiser A, Stehr M, Beyer HJ. Bladder augmentation with small intestinal submucosa leads to unsatisfactory long-term results. J Pediatr Urol. 2013 [Epub ahead of print].

28. Shang K, Rnjak-Kovacina J, Lin Y, Hayden RS, Tao H, Kaplan DL. Accelerated *in vitro* degradation of optically clear low beta-sheet silk films by enzyme-mediated pretreatment. Trans Vis Sci Tech. 2013; 2:2.

29. de Boer WI, Schuller AG, Vermey M, van der Kwast TH. Expression of growth factors and receptors during specific phases in regenerating urothelium after acute injury *in vivo*. Am J Pathol. 1994; 145:1199–1207. [PubMed: 7977650]

30. Kong XT, Dend FM, Hu P, Liang FX, Zhou G, Auerback AB, et al. Roles of uroplakins in plaque formation, umbrella cell enlargement, and urinary tract diseases. J Cell Biol. 2004; 167:1195–1204. [PubMed: 15611339]

31. Uchida W, Masuda N, Shirai Y, Shibasaki K, Satoh N, Takenada T. The role of extracellular Ca2+ in carbachol-induced tonic contraction of the pig detrusor smooth muscle. Naunyn Schmiedebergs Arch Pharmacol. 1994; 350:398–402. [PubMed: 7845476]

32. Hawthorn MH, Chapple CR, Cock M, Chess-Williams R. Urothelium-derived inhibitory factoRs) influences on detrusor muscle contractility *in vitro*. Br J Pharmaco. 2000; 129:416–419.

33. Brading AF, Mostwin JL. Electrical and mechanical responses of guinea-pig bladder muscle to nerve stimulation. Br J Pharmacol. 1989; 98:1083–1090. [PubMed: 2611483]

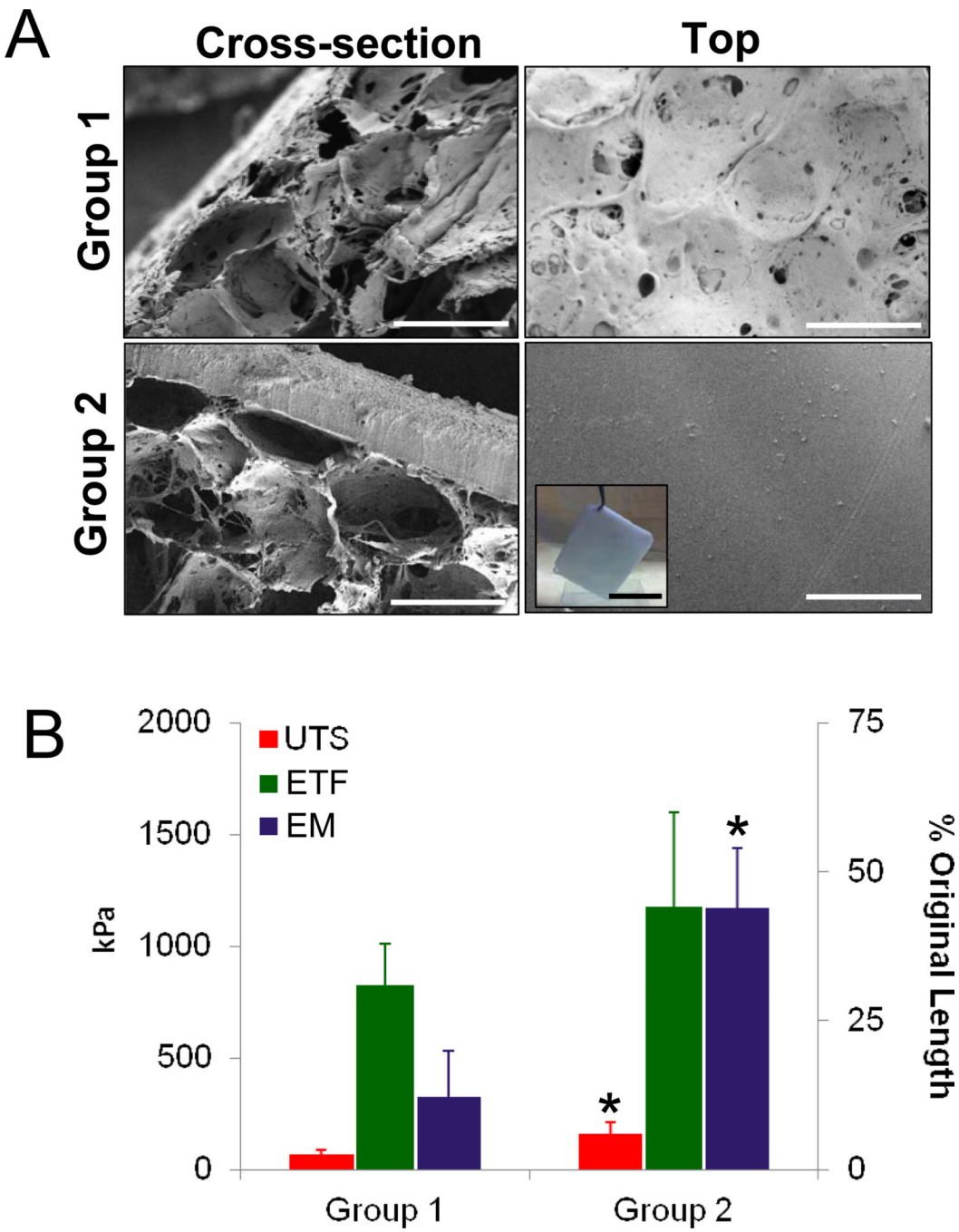

Figure 1.

Structural and mechanical analyses of scaffold groups. [**A**] Photomicrographs of representative SEM images demonstrating cross-sectional and top views of matrix configurations. Scale bar = 400 μm. Inset: gross view of Group 2 scaffold prior to implantation. Scale bar = 4 cm. [**B**] Evaluation of ultimate tensile strength (UTS), elastic modulus (EM), and % elongation to failure (ETF) in matrix groups defined in [A]. Means ± standard deviation per data point. (*) = $p<0.05$ in comparison to Group 1.

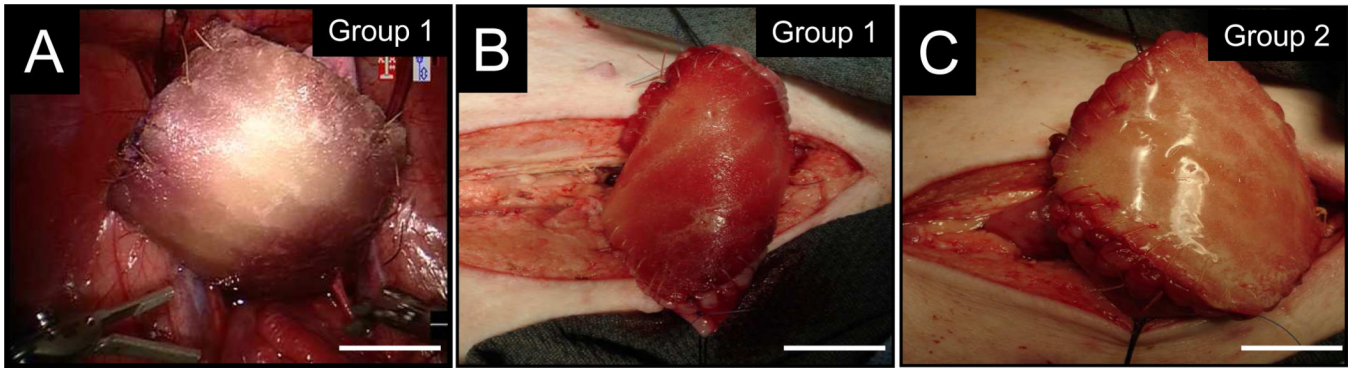

Figure 2.
Porcine augmentation cystoplasty models. Photomicrographs of [**A**] robot-assisted laparoscopic and [**B–C**] open approaches for bladder augmentation with matrix groups. For all panels, scale bars = 2 cm.

A

Pigs	Animal Weight (kg)			Bladder Capacity (ml)			Bladder Compliance (ml/cmH2O)		
	Pre-OP	*3 m*	*% increase*	*Pre-OP*	*3 m*	*% increase*	*Pre-OP*	*3 m*	*% increase*
Group 1									
1	36.8	D	ND	250	D	ND	36.8	D	ND
2	45.1	68.7	52	250	500	100	32	63	95
3	41.2	53	29	200	850	325	38	193	402
4	35	49.9	43	300	1600	433	33	258	691
5	33.6	47	40	400	1400	250	32	109	239
6	35.1	48.4	38	NP	NP	ND	NP	NP	ND
Group 2									
1	37	53.3	44	350	1000	186	17.5	86	393
2	33.4	40.7	22	1000	1650	65	33.4	40.7	22
3	34.3	47.8	39	450	1650	267	34.3	47.8	39
4	36.9	47.5	29	850	1650	94	36.9	47.5	29
Control									
1	37.6	54.7	45	650	1650	154	37.6	54.7	45
2	39	53	36	500	1600	220	39	53	36
3	38.7	55.3	43	1050	1650	57	38.7	55.3	43

B

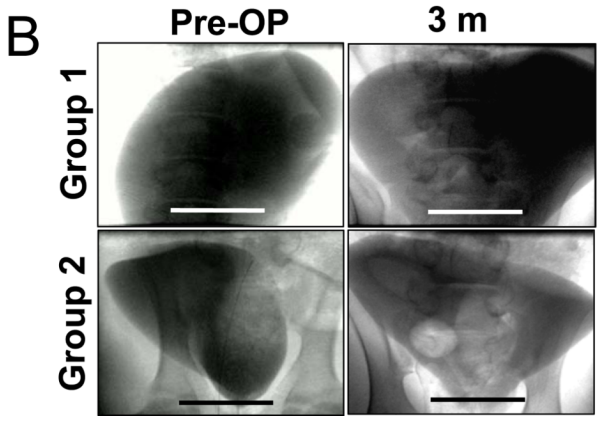

Figure 3.

Animal weight and urodynamic assessments of longitudinal controls and swine augmented with each scaffold group. [**A**] Table of animal weight, bladder capacity and compliance both pre-operatively and following 3 m of matrix implantation. D = animal death prior to scheduled evaluation; NP = evaluation not performed; ND = not determined. [**B**] Photomicrographs of cystograms of swine described in [A]. Scale bar = 6 cm.

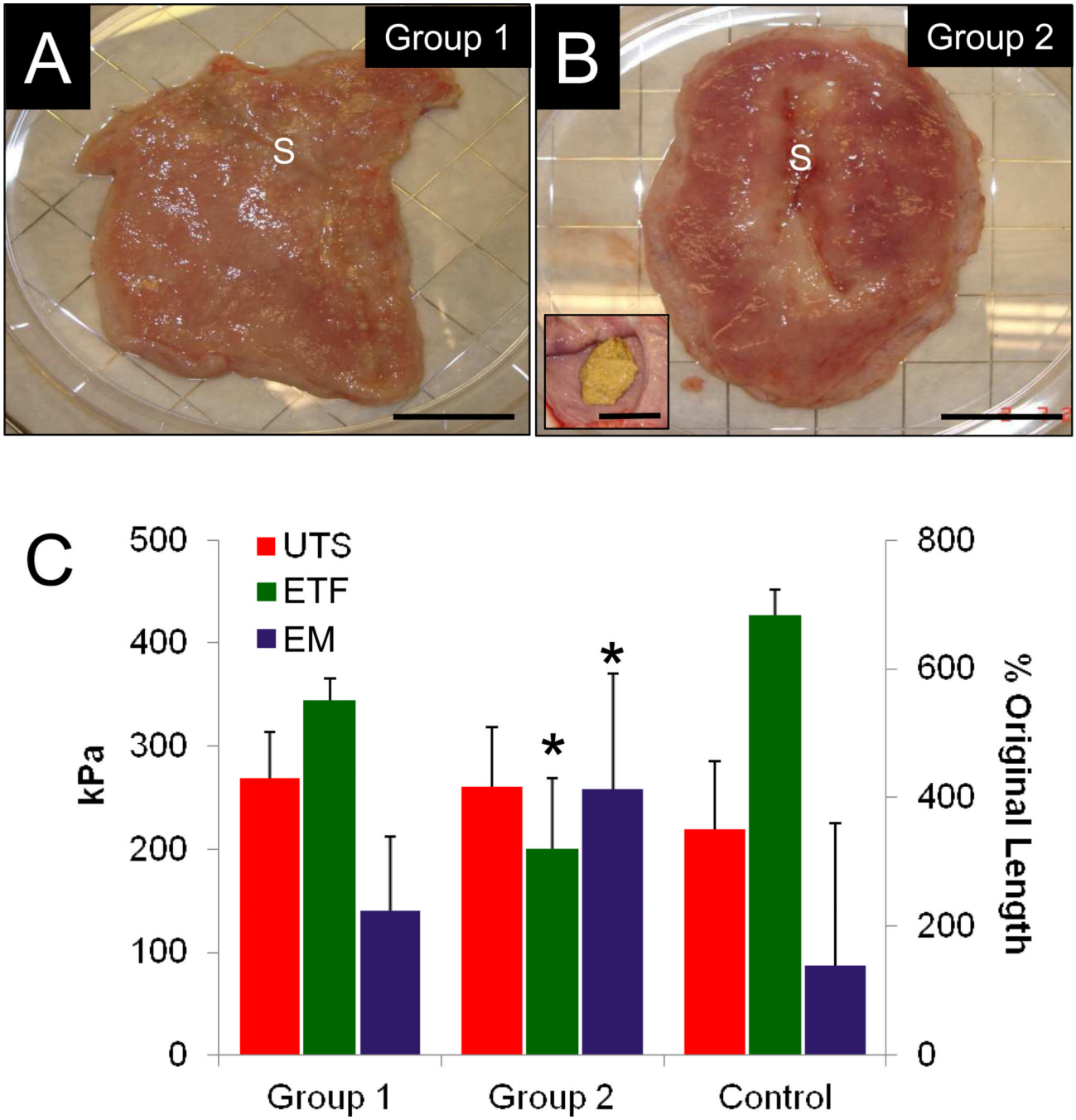

Figure 4.

Gross morphological evaluations and tensile properties of regenerated tissues supported by scaffold groups. [**A**] Photomicrographs of the luminal plane of *de novo* tissue excised from the original scaffold integration site following 3 m of implantation. (S) denotes midline scar. Scale bar = 3 cm. Inset: urinary calculi. Scale bar = 3 cm. [**B**] Evaluation of ultimate tensile strength (UTS), elastic modulus (EM), and % elongation to failure (ETF) in regenerated tissues defined in [A] as well as nonsurgical control bladder specimens. Means ± standard deviation per data point. (*) = $p<0.05$ in comparison to respective control measurements.

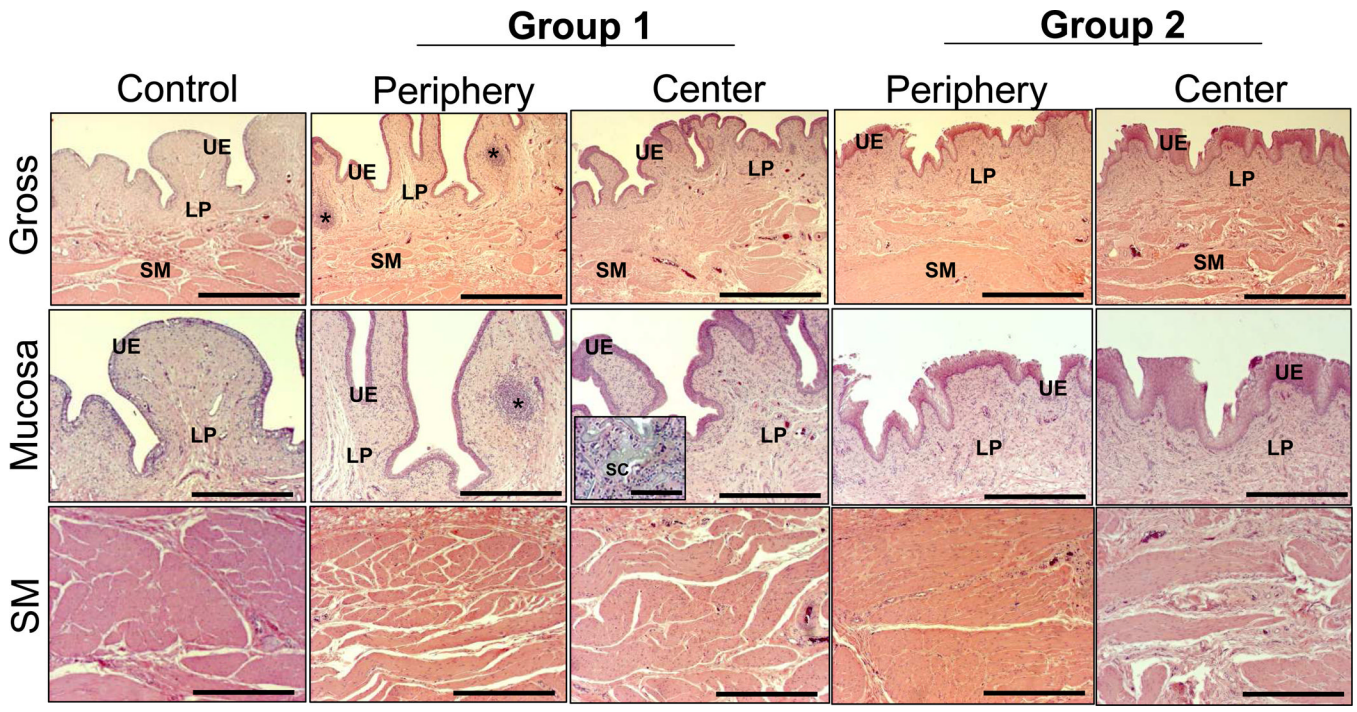

Figure 5.

Cross-sectional histological evaluations (H&E analysis) of radial periphery and central regions of both control and regenerated bladder domes supported by scaffold groups following 3 m of implantation. UE = urothelium; LP = lamina propria; SM = smooth muscle; SC = residual silk scaffold. (*) = aggregates of mononuclear cell infiltrates. Scale bars for 1st row, 800 μm; 2nd–3rd rows, 400 μm; inset, 100 μm.

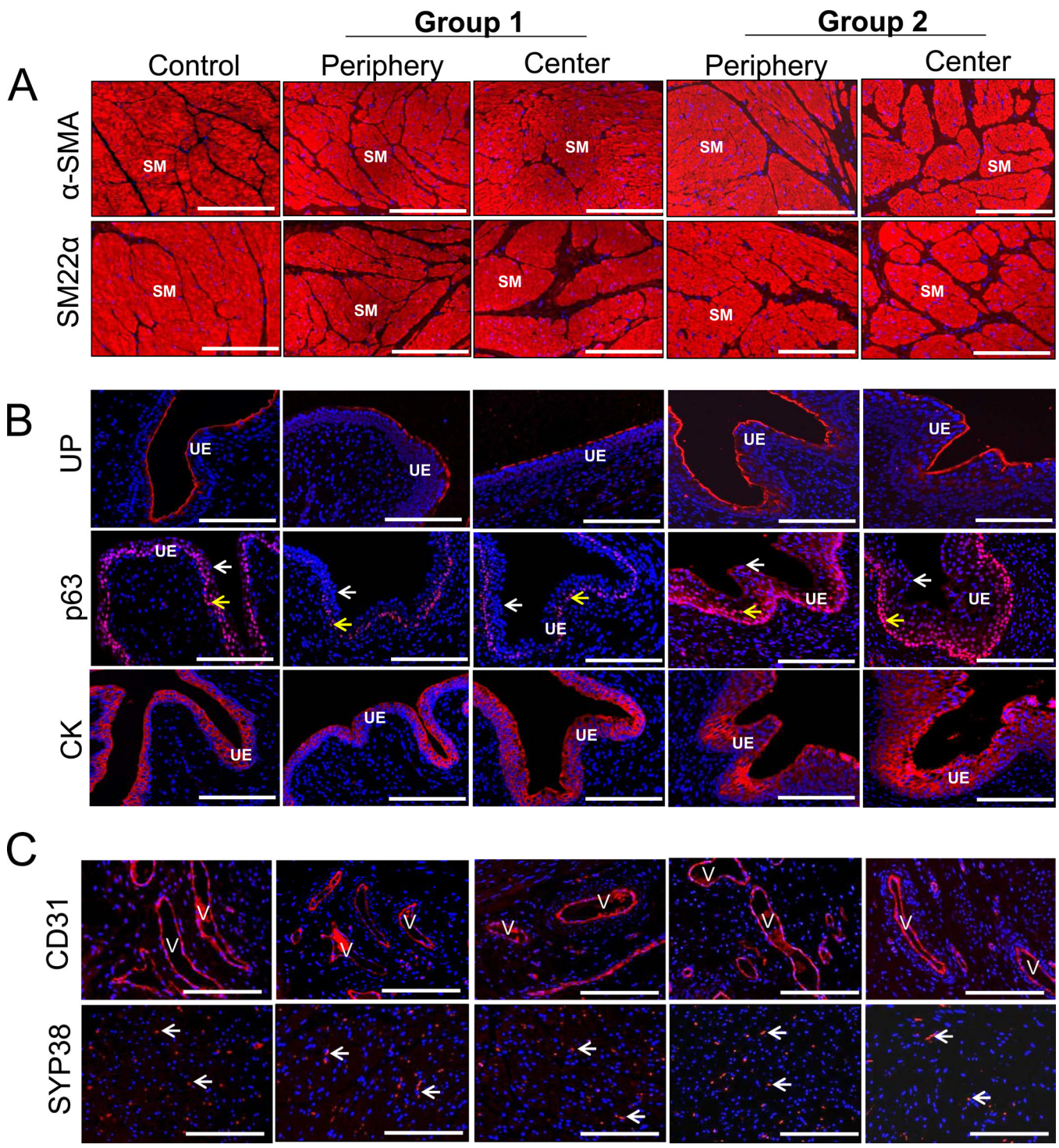

Figure 6.

Immunohistochemical (IHC) assessments of tissue regeneration of radial periphery and central regions of both control and regenerated bladder domes supported by scaffold groups following 3 m of implantation. Photomicrographs of protein expression of [**A**] contractile markers (α-SMA and SM22α); [**B**] urothelial-associated markers, uroplakin (UP), p63, cytokeratins (CK); [**C**] endothelial marker, CD31; and innervation marker, synaptophysin

(SYP38). For [A], SM denotes smooth muscle. For [B] arrows denote p63-positive basal and/or intermediate urothelial cells (yellow); p63-negative superficial urothelial cells (white). For [C], V denotes vessels in top row and white arrows denote neurons in bottom row. For all panels, respective marker expression is displayed in red (Cy3 labeling) and blue denotes DAPI nuclear counterstain. Scale bars in all panels = 200 μm.

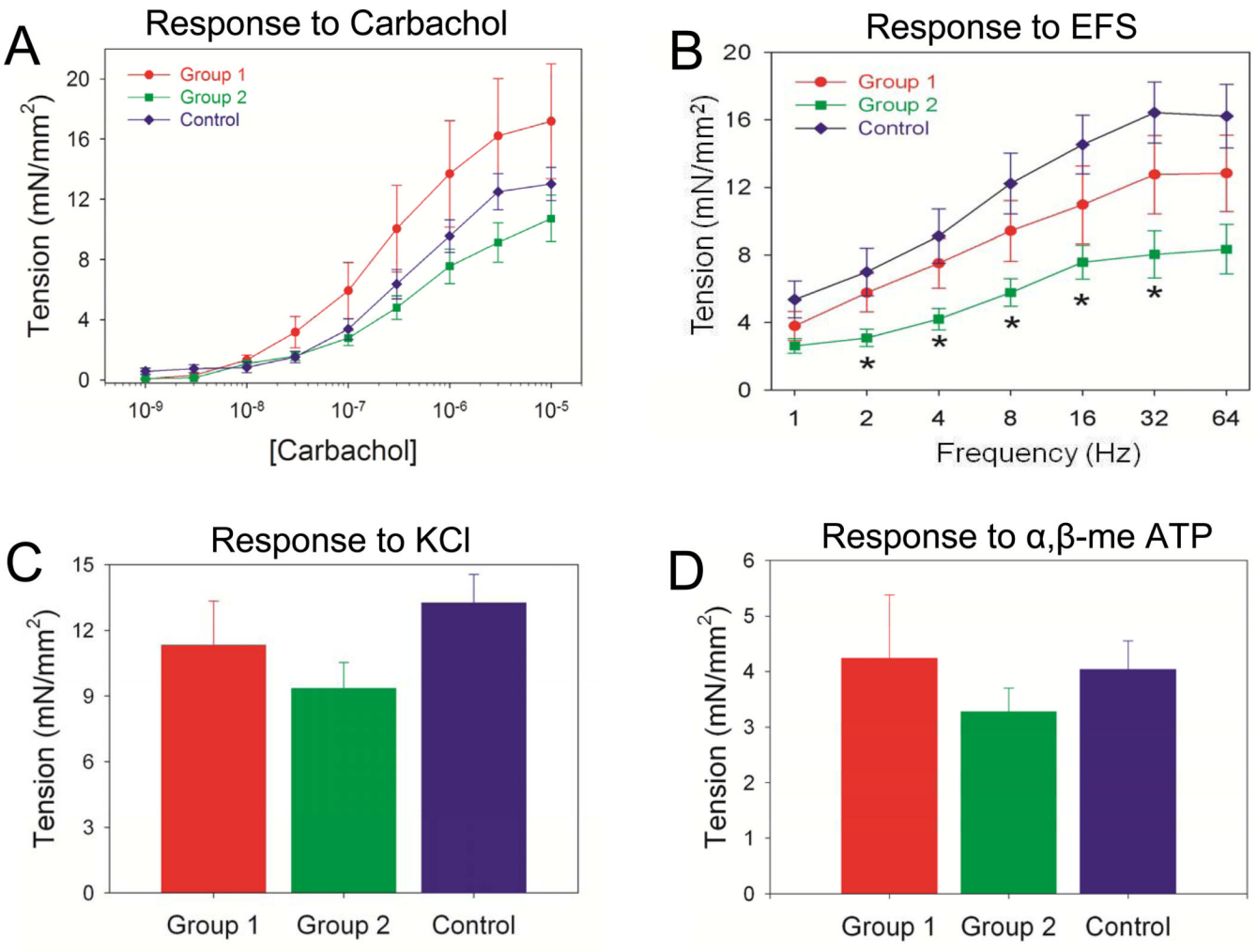

Figure 7.

Ex vivo contractility evaluations of central regions of both control and regenerated bladder domes supported by scaffold groups following 3 m of implantation. [**A**] Dose-response curves for carbachol in denuded bladder strips. [**B**] Frequency response curves for electrical field stimulation (EFS) in specimens described in [A]. (*) = $p<0.05$ in comparison to respective control measurements. Contractile responses to [**C**] increased extracellular KCl (120 mM) and [**D**] α-β-methylene-ATP (10 μM) in samples detailed in [A].